Hindawi
Journal of Chemistry
Volume 2017, Article ID 8579896, 8 pages
https://doi.org/10.1155/2017/8579896

Research Article

A Facile Route to the Preparation of Highly Uniform ZnO@TiO_2 Core-Shell Nanorod Arrays with Enhanced Photocatalytic Properties

Yuanyuan Zhao, Peifei Tong, Dong Ma, Bing Li, Qinzhuang Liu, San Chen, and Yongxing Zhang

Collaborative Innovation Center of Advanced Functional Composites, Huaibei Normal University, Huaibei 235000, China

Correspondence should be addressed to Yongxing Zhang; zyx07157@mail.ustc.edu.cn

Received 14 January 2017; Revised 14 March 2017; Accepted 20 March 2017; Published 11 April 2017

Academic Editor: Roberto Comparelli

Design and synthesis of ZnO@TiO_2 core-shell nanorod arrays as promising photocatalysts have been widely reported. However, it remains a challenge to develop a low-temperature, low-cost, and environmentally friendly method to prepare ZnO@TiO_2 core-shell nanorod arrays over a large area for future device applications. Here, a facile, green, and efficient route is designed to prepare the ZnO@TiO_2 nanorod arrays with a highly uniform core-shell structure over a large area on Zn wafer via a vapor-thermal method at relatively low temperature. The growth mechanism is proposed as a layer-by-layer assembly. The photocatalytic decomposition reaction of methylene blue (MB) reveals that the ZnO@TiO_2 core-shell nanorod arrays have excellent photocatalytic activities when compared with the performance of the ZnO nanorod arrays. The improved photocatalytic activity could be attributed to the core-shell structure, which can effectively reduce the recombination rate of electron-hole pairs, significantly increase the optical absorption range, and offer a high density of surface active catalytic sites for the decomposition of organic pollutants. In addition, it is very easy to separate or recover ZnO@TiO_2 core-shell nanorod array catalysts when they are used in water purification processes.

1. Introduction

In recent years, there has been increasing interest in the design and synthesis of ZnO@TiO_2 core-shell nanorod arrays to improve the quantum efficiency of Dye-Sensitized Solar Cells (DSSC), highly transparent self-cleaning coating for LEDs, and photocatalysts for the decomposition of organic pollutants in waste water [1–10]. This is mainly attributed that the large binding energy of ZnO and the high reactivity of TiO_2 can significantly increase the process of electron and hole transfer between the corresponding conduction and valence bands. Thus, compared with photoanode materials or single metal oxide catalysts [11–18], a better separation of photogenerated carriers can be obtained in ZnO@TiO_2 core-shell structures.

Until now, several types of ZnO@TiO_2 core-shell nanorod arrays are fabricated by different methods. Typically, Wang et al. have prepared ZnO/TiO_2 core-shell nanorod arrays by a plasma sputtering decoration route [19]. Heterostructure ZnO/TiO_2 core-brush nanostructures are synthesized on glass substrates by a combination of aqueous solution growth and magnetron sputtering method [6, 20]. Greene et al. have reported that the TiO_2 shells are grown on the ZnO nanorod arrays in a traveling-wave atomic layer deposition (ALD) system using $TiCl_4$ and water at 300°C with a process pressure of 300–500 mTorr [21]. All the ZnO@TiO_2 core-shell nanorod arrays in the above-mentioned reports are obtained under severe conditions (including low pressure, relatively high temperature, and anaerobic conditions); and special equipment is required. Thus, it remains a challenge to develop a low-temperature, low-cost, and environmentally friendly method to prepare ZnO@TiO_2 core-shell nanorod arrays over a large area for future device applications.

Herein, a facile, green, and efficient route is proposed to achieve a decoration of ZnO nanorod arrays with TiO_2 nanoparticle via a vapor-thermal method at relatively low

temperature. And the morphology of the $ZnO@TiO_2$ nanorod arrays obtained heterostructure shows a core-shell arrangement with a highly uniform over a large area on Zn wafer. A 60 mL stainless steel autoclave with a Teflon liner is used to achieve the preparation process, which is simpler equipment than magnetron sputtering system and ALD system that had been widely used previously. The growth mechanism of the $ZnO@TiO_2$ nanorod arrays is discussed. The high UV light photocatalytic efficiency of the product is achieved via heterojunction effect. And the advantages of $ZnO@TiO_2$ heterostructures have the following features: (a) the $ZnO@TiO_2$ core-shell structure heterojunction can improve electron-charge separation efficiency. So, the proposed route to prepare the $ZnO@TiO_2$ core-shell nanorod arrays represents a significant advance for the degradation of organic pollutants in water; (b) compared with some nanoscale catalyst particles, the $ZnO@TiO_2$ film with a core-shell structure has unique advantages for practical applications from the aspect of long life, low-cost, and high degradation efficiency. Particularly, when TiO_2 nanoparticles are coated on the surface of ZnO nanorod arrays, it is very convenient to separate or recover them in water purification processes; (c) ZnO is sensitive to both acidic and basic solutions (chemical corrosion). However, when the outer TiO_2 layers are formed on the surface of ZnO nanorod arrays, they can serve as protective layers in solutions.

2. Experimental

2.1. Preparation of Highly Uniform $ZnO@TiO_2$ Core-Shell Nanorod Arrays. All reagents were purchased from Sinopharm Chemical Reagent Co., Ltd. (China). The reagents were of analytical grade and used without further purification. The $ZnO@TiO_2$ nanorod arrays on Zn wafer were prepared by following two steps: firstly, a piece of zinc wafer (1 cm × 1 cm, 99.99%) pretreated by sonication in ethanol and deionized water and dried in air was placed in a sealed bottle containing of zinc nitrate hydrate (0.1 M) and hexamethylenetetramine (0.1 M) for three hours at 75°C. The ZnO nanorod arrays were obtained. The samples were rinsed with deionized water for several times and dried at 60°C for several hours before being used [22]. Secondly, the $ZnO@TiO_2$ nanorod arrays on Zn wafer were prepared by the vapor-thermal method using tetrabutyl titanate (TBOT) as the titanium source. In a typical procedure, the piece of zinc wafer with ZnO nanorod arrays (1 cm × 1 cm) was placed 10 mL beaker with the mixture of ethanol and TBOT. Then, the beaker was placed into a 60 mL stainless steel autoclave with a Teflon liner. The free space between the Teflon liner and the beaker was filled with distilled water. After sealing, the autoclave was heated to 150°C for 6 h. At the end of the reaction, the autoclave was cooled naturally to room temperature, and the products were collected and washed for three cycles using deionized water and ethanol, respectively. And then, they were dried at 50°C in a vacuum oven for 3 h.

2.2. Characterization. The surface morphologies of the products were examined by Field emission scanning electron microscope (FESEM, Quanta 200 FEG). Transmission electron microscopy (TEM), high resolution transmission electron microscope (HRTEM) images, and selected area energy dispersive X-ray spectrum (EDS) were obtained on a JEOL-2012 TEM coupled with an EDS detector, operated at an acceleration voltage of 200 kV. The UV-Vis spectra were measured by a UV/Vis/NIR spectrophotometer (Hitachi U-4100).

2.3. Photocatalytic Properties. In our experiments, photocatalytic decomposition of MB under UV light illumination has been conducted at room temperature. Both the ZnO nanorod arrays and $ZnO@TiO_2$ nanorod arrays grown on Zn wafer with size 1 cm × 1 cm were soaked into two identical bottles containing methylene blue (MB, 10 mL, 1×10^{-5} M). Before UV light illumination (λ: 254 nm, output power: 8 W, the irradiance of the UV light source is 20 $\mu W/cm^2$), they were stored in the dark for 30 min to ensure the establishment of an adsorption equilibrium for MB at ambient temperature. In addition, in order to ensure that both the samples could receive the same amount of UV illumination, they were placed 5 cm away from the UV light sources in our experiments. As a comparison, one bottle containing blank MB solution was also carried out under the same condition. The concentrations of MB in the above three bottles at given time intervals were determined using a UV/Vis/NIR spectrophotometer (Hitachi U-4100).

3. Results and Discussion

Figures 1(a) and 1(b) show scanning electron microscope (SEM) images of the ZnO nanorod arrays grown on Zn wafer. The low-magnification SEM image (Figure 1(a)) shows a large area uniform film-like structure deposited on the wafer. From the high-magnification SEM image (Figure 1(b)), it is clear that high density ZnO nanorod arrays are grown vertically on the ZnO wafer. These nanorods have a nearly uniform diameter of 180–200 nm. The inset in Figure 1(b) is the TEM image of a single ZnO nanorod with length about 1.4 μm. From the image, it is confirmed that the diameter of ZnO nanorod is about 190 nm. Figures 1(c) and 1(d) show SEM images of the $ZnO@TiO_2$ nanorod arrays grown on the surface of the Zn wafer. The low-magnification image (Figure 1(c)) also displays a large scale uniform film-like structure grown on the ZnO wafer. Figure 1(d) shows the high-magnification SEM image of $ZnO@TiO_2$ nanorod arrays, from which it displays that high density $ZnO@TiO_2$ nanorod arrays with the diameter of about 230–260 nm are grown vertically on the surface of the ZnO wafer. From the high-magnification images (Figures 1(b) and 1(c)), it is clear that the diameter of $ZnO@TiO_2$ nanorod is obviously larger than that of ZnO nanorod.

The high-magnification SEM image shown in Figure 2(a) further observes the detailed structures of $ZnO@TiO_2$ nanorod arrays. It seems that the $ZnO@TiO_2$ nanorods have core-shell structures (the black and white arrows indicate the shell structure and the core structure, resp.). In addition, the open tip of $ZnO@TiO_2$ nanorod shown in Figure 2(a) reveals the top of ZnO nanorod structure (indicated by the black dotted circle). Figure 2(b) shows that the inner edge of the

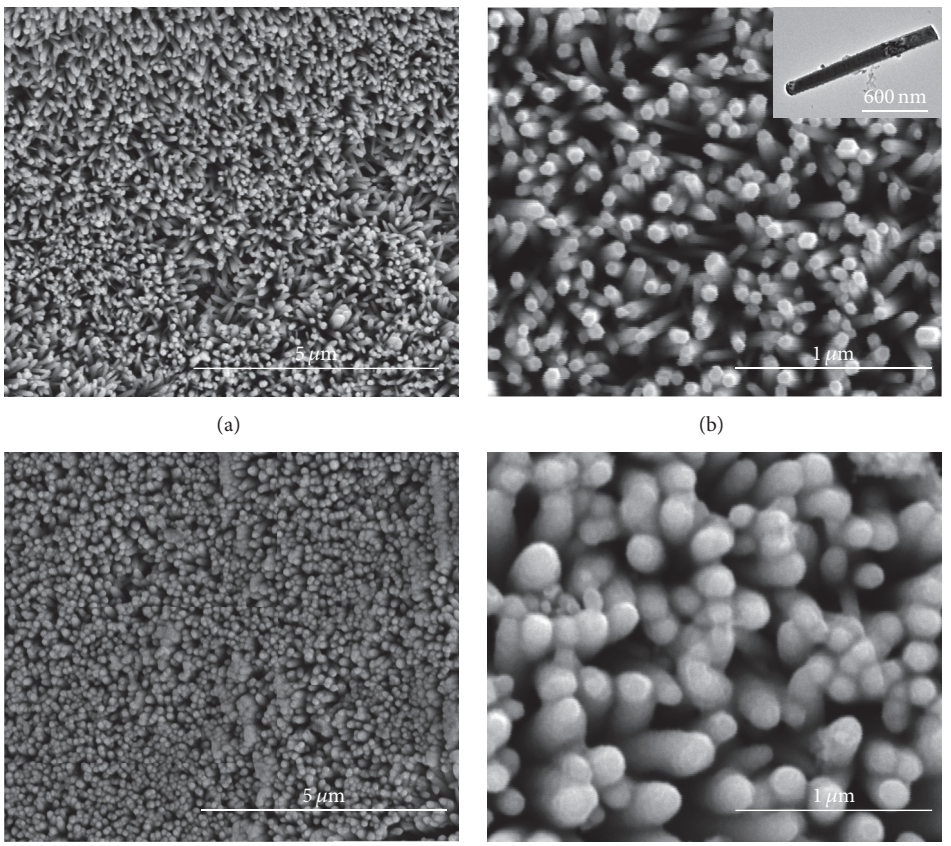

Figure 1: SEM (a) and high resolution SEM (b) of ZnO nanorod arrays (inset of Figure (b): TEM of ZnO nanorod); SEM (c) and high resolution SEM (d) of ZnO@TiO_2 nanorod arrays.

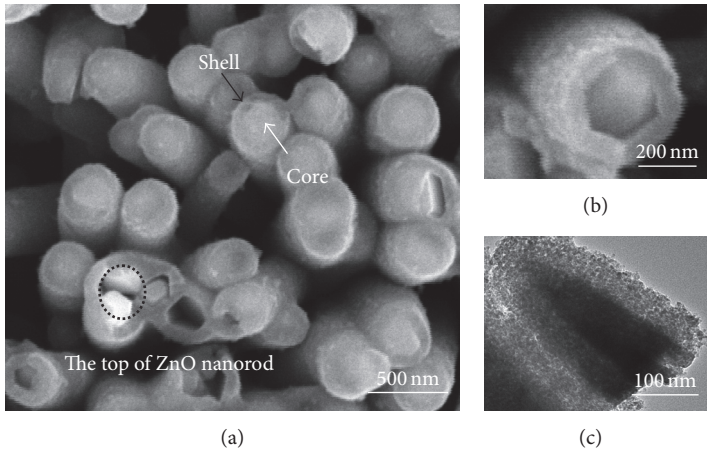

Figure 2: High resolution SEM ((a) and (b)) and TEM (c) of ZnO@TiO_2 nanorod.

TiO_2 shell and the outer edge of ZnO core have hexagonal structures. The thickness of the TiO_2 shell is about 40–60 nm. The TEM image shown in Figure 2(c) clearly confirms that the ZnO@TiO_2 nanorod has core-shell structure. The TiO_2 shell thickness of 50 nm is consistent with the result of the observation from Figure 2(b).

Figure 3 shows the TEM image and the corresponding energy dispersive spectroscopic (EDS) analysis of ZnO@TiO_2 nanorod. In the top right corner of Figure 3(a), the lattice fringe spacing of 0.525 nm observed from the HRTEM image corresponded to the (001) plane of hexagonal ZnO phase (JCPDS card number 00-005-0664, space group: P63mc

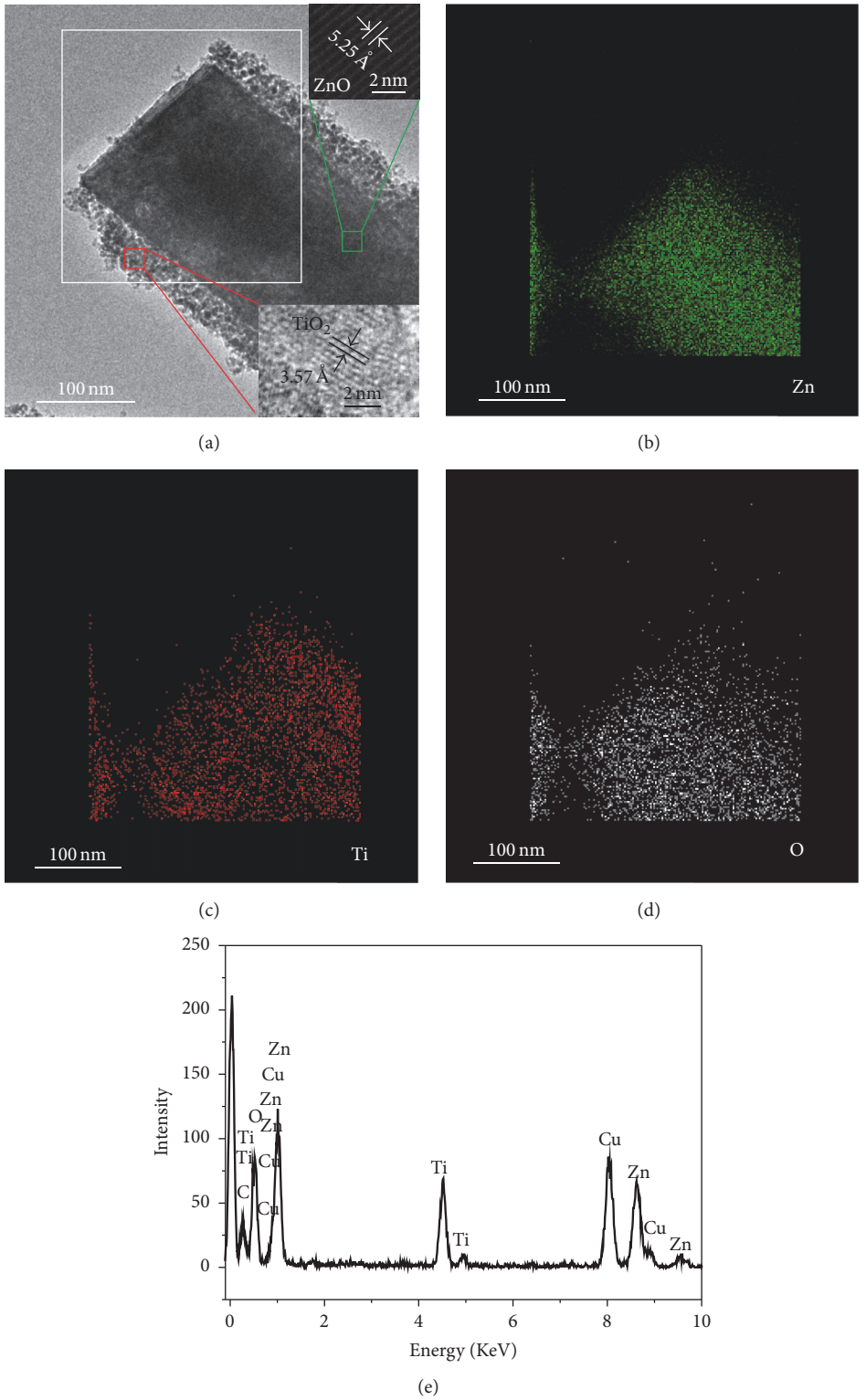

FIGURE 3: (a) TEM images of $ZnO@TiO_2$ nanorod (Inset: HRTEM image of ZnO and TiO_2). Electron energy loss: (b) Zn, (c) Ti, and (d) O element mapping images of the $ZnO@TiO_2$ nanorod. (e) EDS data of the $ZnO@TiO_2$ nanorod.

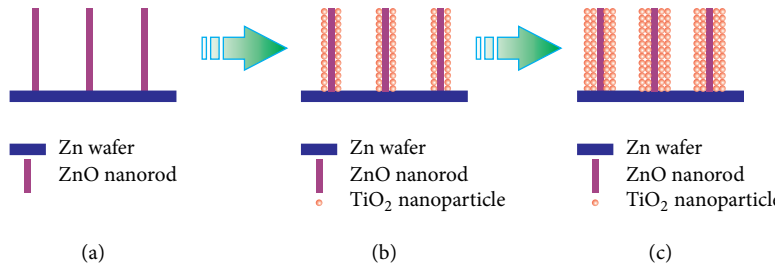

Figure 4: The growth mechanism of the ZnO@TiO_2 nanorod.

(186)) with *c*-axial growth direction. The hexagonal ZnO phase is identical with the reported ones [22]. The lattice fringe spacing of 0.357 nm observed from the HRTEM image corresponded to the (101) plane of anatase TiO_2 phase in the bottom right corner of Figure 3(a) (JCPDS card number 00-021-1272, space group: I41/amd (141)). This result is consistent with that reported previously [23]. In order to further confirm the presence of both TiO_2 and ZnO components in the ZnO@TiO_2 nanorods, electron mapping image analysis is used to analyze the sample (Figures 3(a)–3(d)). The electron mapping images can be obtained via visualizing the inelastically scattered electrons in the energy loss windows for elemental Zn, Ti, and O. The different color areas displayed in Figures 3(a)–3(d) indicate Zn-, Ti-, and O-enriched areas of the sample, respectively, which indicate the presence of both ZnO and TiO_2 in the ZnO@TiO_2 nanorods. The images also show that the ZnO@TiO_2 nanorod has very good uniform core-shell structures. The EDS analysis (Figure 3(e)) of the ZnO@TiO_2 nanorods indicates the existence of Zn, Ti, and O elements (copper signals are present from the copper grid support).

The growth mechanism of the ZnO@TiO_2 nanorod arrays can be described as follows. During the experiment, the ethanol evaporates firstly when the reaction system is heated. It is mainly due to the fact that the ethanol has a lower boiling point than water. And then, the water vapor promotes the hydrolysis of TBOT dissolved in ethanol. It is supposed that there are many nucleation sites on the surface of the ZnO nanorod. During the initial stage, TiO_2 nanoparticles formed by hydrolysis of TBOT are deposited on the nucleation site of the ZnO surface. With the passage of reaction time (Figure 4(b)), the as-formed TiO_2 nanoparticles subsequently serve as nucleation sites for further deposition of TiO_2 nanoparticles (Figure 4(c)), which lead to layer-by-layer assembly.

Figure 5(a) shows the typical diffuse reflectance spectra (DRS) for ZnO nanorod arrays and ZnO@TiO_2 nanorod arrays at room temperature. As shown in curve 1 of Figure 5(a), ZnO nanorod arrays present a continuous wide absorption band in the UV light region. When TiO_2 shell is formed on the surface of ZnO nanorod arrays (ZnO@TiO_2 nanorod arrays), the increase in peak intensity can be observed obviously (as shown in curve 2 of Figure 5(a)). In the UV region, from 200 to 320 nm, the peak intensity in continuous UV absorption band is stronger than that of ZnO nanorod arrays. The changes of UV peak intensity may be affected by scattering, particle size, aggregates, and so on [24]. In addition, as shown in Figure 5(a), a red shift of the band gap absorption edge can also be observed in the $\lambda > 320$ nm region. To determine the band gaps of the ZnO@TiO_2 nanorod heterostructures, we replotted the spectra shown in Figure 5(a) in the form shown in the inset image of Figure 5(a) obtained by the application of the Kubelka-Munch algorithm [14]. From the inset image of Figure 5(a), the estimated band gap of the ZnO@TiO_2 is 2.95 eV, which is smaller than that of ZnO 3.01 eV. This may be due to the formation of a ZnO@TiO_2 heterojunction slowing the electron-hole recombination and hence reducing the level of emission. Thus, the photocatalytic ability of the ZnO@TiO_2 heterostructures is improved, which is demonstrated by the following photocatalytic experiments.

As shown in Figure 5(b), the MB decomposition rates of the samples are compared over a period of time. The MB decomposition rate in the bottle containing blank MB solution with catalysts is only about 12% after 200 min of photocatalytic reaction. However, 60% and 86% of MB concentration are decomposed by the ZnO nanorod arrays and ZnO@TiO_2 nanorod arrays grown on Zn wafer, respectively. The ZnO@TiO_2 nanorod arrays grown on Zn wafer show superior photocatalytic activity to the ZnO nanorod arrays grown on Zn wafer. This can be attributed to the formation of the P-N core-shell heterojunction between ZnO and TiO_2. The P-N core-shell heterojunction can enhance the charge separation effect under UV illumination. Thus, the composite nanostructures can further promote the photocatalytic activity [6, 11, 25, 26]. In addition, the comparison with the photocatalytic activity of the conventional benchmark (TiO_2 P25 Evonik) has also been investigated. From Figure 5(b), it is clear that the photocatalytic degradation capacity of TiO_2 (P25 Evonik) particles is higher than that of the ZnO@TiO_2 films with a core-shell structure. However, compared with TiO_2 (P25 Evonik) particles, the ZnO@TiO_2 films with a core-shell structure have unique advantages for practical applications. It is very convenient to separate or recover them in water purification processes when TiO_2 nanoparticles are coated on the surface of ZnO nanorod arrays.

The photocatalytic durability of the ZnO@TiO_2 nanorod arrays is also tested. Figure 5(c) displays the cyclic photodegradation of MB using ZnO@TiO_2 nanorod arrays. After fifteen cycles, the ZnO@TiO_2 nanorod arrays still maintain high photocatalytic ability. The core-shell structures of the

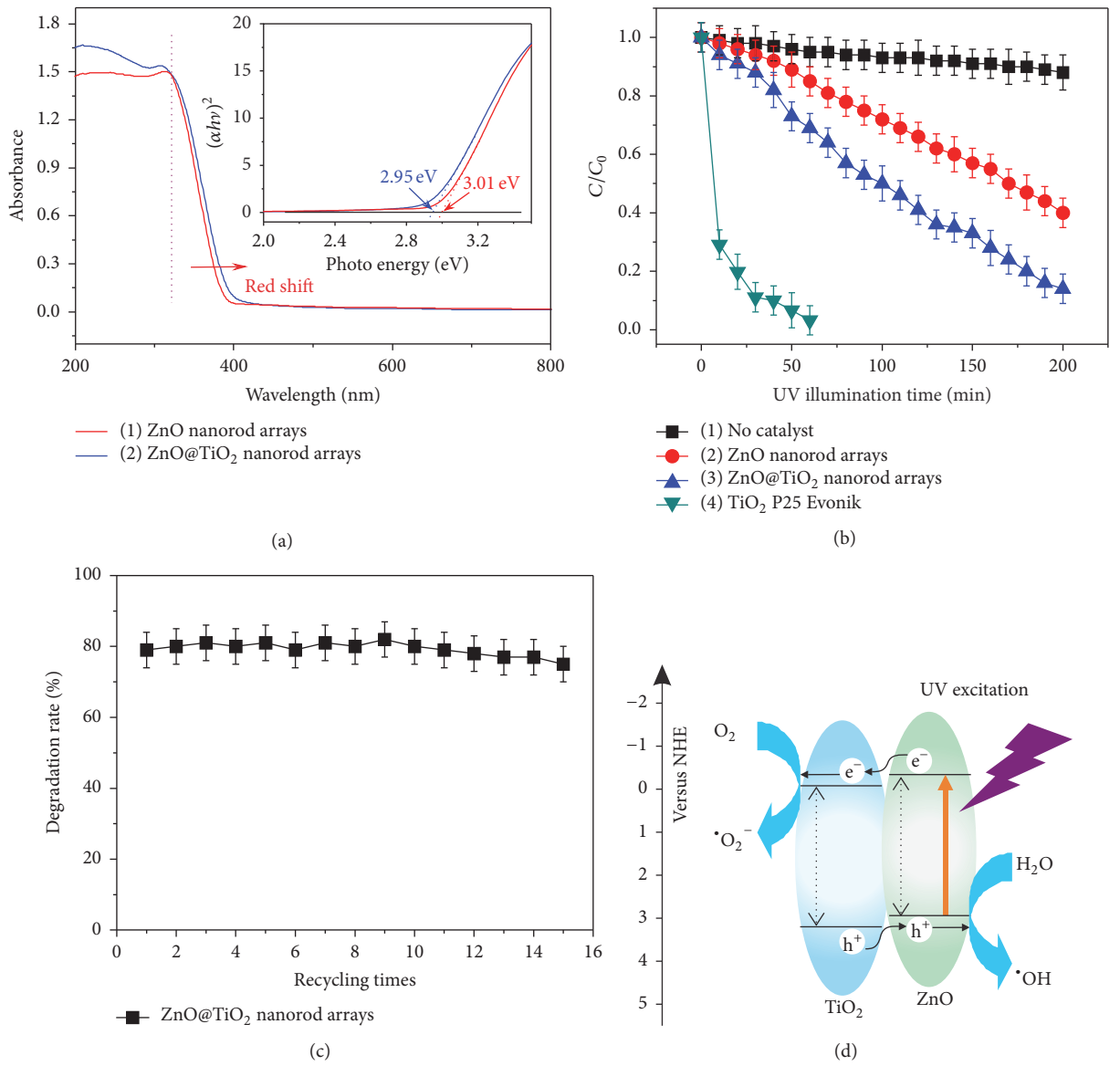

FIGURE 5: (a) Diffuse reflectance spectra (DRS) and (inset) plot of transferred Kubelka-Munch versus energy of the light absorbed for the ZnO nanorod arrays and ZnO@TiO_2 nanorod arrays. (b) Comparison of photocatalytic decomposition rates of MB with different catalysts. (c) Cyclic photodegradation of MB using ZnO@TiO_2 nanorod arrays. The same ZnO@TiO_2 nanorod arrays for degradation of MB are tested up to 15 cycles. The photocatalytic time is 180 min for each cycle. (d) Photogenerated electron transfer process in the ZnO@TiO_2 nanorod under UV illumination. The scale bars represent the standard deviations of three replicated samples.

ZnO@TiO_2 nanorod arrays are expected to have a long service life. Actually, in our sample, ZnO is sensitive to both acidic and basic solutions (chemical corrosion). However, when the outer TiO_2 layers are formed on the surface of ZnO nanorod arrays, they can serve as protective layers in solutions. Furthermore, the photocorrosion of ZnO under UV illumination can also be prevented by TiO_2 layers. Photocorrosion is a very important shortcoming for photocatalysts such as CdS and ZnO but not for TiO_2 [27, 28]. Thus, these uniform core-shell structures of ZnO@TiO_2 nanorod arrays can obviously improve the efficiency and stability of the photocatalyst.

The photocatalytic mechanism of ZnO@TiO_2 nanorod arrays for MB is displayed in Figure 5(d). Under UV illumination, both ZnO and TiO_2 can absorb the photons. Thus, the electron (e^-) and hole (h^+) are obtained. The produced e^- transfers from the conduction band (CB) ZnO to TiO_2, while h^+ transfers from the valence band (VB) of TiO_2 to ZnO. As a result, an efficient separation of photogenerated electron and hole pairs at the core-shell heterojunction interface of ZnO and TiO_2 is reached [29]. These electron and hole pairs improve the occurrence of redox processes; electrons reduce dissolved O_2 to $^{\bullet}O_2^-$, while h^+ forms $HO^{\bullet}$. Thus, MB molecules will be easily decomposed into CO_2 and H_2O by the

strong oxidizer-reducer through some oxidation-reduction reactions.

4. Conclusion

In summary, we have reported a facile, green, efficient method for the preparation of ZnO@TiO_2 core-shell nanorod arrays grown on Zn wafer. The product has highly uniform structures over a large area. It is shown that the product has excellent photocatalytic activities for the degradation of MB under UV light illumination when compared with the performance of the ZnO nanorod arrays grown on Zn wafer. This is because the ZnO@TiO_2 core-shell structure heterojunction can improve electron-charge separation efficiency. So, the proposed route to prepare the ZnO@TiO_2 core-shell nanorod arrays represents a significant advance for the degradation of organic pollutants in water. In addition, compared with some nanoscale catalyst particles, the ZnO@TiO_2 film with a core-shell structure has unique advantages for practical applications from the aspect of long life low-cost and high degradation efficiency. When TiO_2 nanoparticles are coated on the surface of ZnO nanorod arrays, it is very convenient to separate or recover them in water purification processes. Recycling of photocatalyst in nanometer scale from the environmental system is an important focus in practical applications [30]. So, our proposed route to prepare ZnO@TiO_2 core-shell structure catalysts represents a very important advance for environmental remediation applications.

Conflicts of Interest

The authors declare that there are no conflicts of interest regarding the publication of this paper.

Acknowledgments

This research was supported by the National Natural Science Foundation of China (51302102 and 11504120), the Natural Science Foundation of Anhui Province (1708085ME96), the Key Natural Science Research Project for Colleges and Universities of Anhui Province (KJ2016A638 and KJ2016SD51), the Huaibei Scientific Talent Development Scheme (20140305 and 20140318), and the Huaibei Normal University Youth Research Project (2014xq017).

References

[1] X. Li, J. Zhu, and B. Wei, "Hybrid nanostructures of metal/two-dimensional nanomaterials for plasmon-enhanced applications," *Chemical Society Reviews*, vol. 45, no. 11, pp. 3145–3187, 2016.

[2] Y. Zhang, Y. Ye, X. Zhou et al., "Monodispersed hollow aluminosilica microsphere@hierarchical γ-AlOOH deposited with or without $Fe(OH)_3$ nanoparticles for efficient adsorption of organic pollutants," *Journal of Materials Chemistry A*, vol. 4, no. 3, pp. 838–846, 2016.

[3] S. Guo, X. Li, J. Zhu, T. Tong, and B. Wei, "Au NPs@MoS_2 submicrometer sphere-ZnO nanorod hybrid structures for efficient photocatalytic hydrogen evolution with excellent stability," *Small*, vol. 12, no. 41, pp. 5692–5701, 2016.

[4] M.-H. Yeh, L.-Y. Lin, C.-Y. Chou et al., "Preparing core-shell structure of ZnO@TiO2 nanowires through a simple dipping-rinse-hydrolyzation process as the photoanode for dye-sensitized solar cells," *Nano Energy*, vol. 2, no. 5, pp. 609–621, 2013.

[5] D. Guo, J. Wang, C. Cui et al., "ZnO@TiO2 core-shell nanorod arrays with enhanced photoelectrochemical performance," *Solar Energy*, vol. 95, pp. 237–245, 2013.

[6] X. Yan, C. Zou, X. Gao, and W. Gao, "ZnO/TiO2 core-brush nanostructure: processing, microstructure and enhanced photocatalytic activity," *Journal of Materials Chemistry*, vol. 22, no. 12, pp. 5629–5640, 2012.

[7] M. Law, L. E. Greene, A. Radenovic, T. Kuykendall, J. Liphardt, and P. Yang, "ZnO-Al2O3 and ZnO-TiO2 core-shell nanowire dye-sensitized solar cells," *Journal of Physical Chemistry B*, vol. 110, no. 45, pp. 22652–22663, 2006.

[8] M. Wang, C. Huang, Y. Cao et al., "The effects of shell characteristics on the current-voltage behaviors of dye-sensitized solar cells based on ZnO/TiO_2 core/shell arrays," *Applied Physics Letters*, vol. 94, no. 26, Article ID 263506, 2009.

[9] R. Wang, H. Tan, Z. Zhao et al., "Stable ZnO@TiO2 core/shell nanorod arrays with exposed high energy facets for self-cleaning coatings with anti-reflective properties," *Journal of Materials Chemistry A*, vol. 2, no. 20, pp. 7313–7318, 2014.

[10] H. M. A. Javed, W. Que, X. Yin, Y. Xing, J. Shao, and L. B. Kong, "ZnO/TiO2 nanohexagon arrays heterojunction photoanode for enhancing power conversion efficiency in dye-sensitized solar cells," *Journal of Alloys and Compounds*, vol. 685, pp. 610–618, 2016.

[11] F. Kayaci, S. Vempati, C. Ozgit-Akgun, I. Donmez, N. Biyikli, and T. Uyar, "Selective isolation of the electron or hole in photocatalysis: ZnO-TiO2 and TiO2-ZnO core-shell structured heterojunction nanofibers via electrospinning and atomic layer deposition," *Nanoscale*, vol. 6, no. 11, pp. 5735–5745, 2014.

[12] M. Pazoki, N. Nafari, and N. Taghavinia, "Ab initio study of electronic effects in the ZnO/TiO2 core/shell interface: application in dye sensitized solar cells," *RSC Advances*, vol. 4, no. 1, pp. 301–307, 2014.

[13] D. Barreca, E. Comini, A. P. Ferrucci et al., "First example of ZnO-TiO2 nanocomposites by chemical vapor deposition: structure, morphology, composition, and gas sensing performances," *Chemistry of Materials*, vol. 19, no. 23, pp. 5642–5649, 2007.

[14] R. S. Mane, W. J. Lee, H. M. Pathan, and S.-H. Han, "Nanocrystalline TiO2/ZnO thin films: fabrication and application to dye-sensitized solar cells," *Journal of Physical Chemistry B*, vol. 109, no. 51, pp. 24254–24259, 2005.

[15] J. Ren, W. Que, X. Yin, Y. He, and H. M. A. Javed, "Novel fabrication of TiO2/ZnO nanotube array heterojunction for dye-sensitized solar cells," *RSC Advances*, vol. 4, no. 15, pp. 7454–7460, 2014.

[16] C. Lévy-Clément, R. Tena-Zaera, M. A. Ryan, A. Katty, and G. Hodes, "CdSe-sensitized p-CuSCN/nanowire n-ZnO heterojunctions," *Advanced Materials*, vol. 17, no. 12, pp. 1512–1515, 2005.

[17] Z. Lou, J. Deng, L. Wang, R. Wang, T. Fei, and T. Zhang, "A class of hierarchical nanostructures: ZnO surface-functionalized TiO2 with enhanced sensing properties," *RSC Advances*, vol. 3, no. 9, pp. 3131–3136, 2013.

[18] J. Arin, S. Thongtem, and T. Thongtem, "Single-step synthesis of ZnO/TiO2 nanocomposites by microwave radiation and their photocatalytic activities," *Materials Letters*, vol. 96, pp. 78–81, 2013.

[19] M. Wang, C. Huang, Y. Cao et al., "A plasma sputtering decoration route to producing thickness-tunable ZnO/ TiO_2 core/shell nanorod arrays," *Nanotechnology*, vol. 20, no. 28, Article ID 285311, 2009.

[20] C. W. Zou, X. D. Yan, J. Han et al., "Preparation and enhanced photoluminescence property of ordered ZnO/TiO2 bottlebrush nanostructures," *Chemical Physics Letters*, vol. 476, no. 1–3, pp. 84–88, 2009.

[21] L. E. Greene, M. Law, B. D. Yuhas, and P. Yang, "ZnO—TiO2 core—shell nanorod/P3HT solar cells," *Journal of Physical Chemistry C*, vol. 111, no. 50, pp. 18451–18456, 2007.

[22] M. Wang, C.-H. Ye, Y. Zhang et al., "Synthesis of well-aligned ZnO nanorod arrays with high optical property via a low-temperature solution method," *Journal of Crystal Growth*, vol. 291, no. 2, pp. 334–339, 2006.

[23] Y. Su, J. Yu, and J. Lin, "Vapor-thermal preparation of highly crystallized TiO_2 powder and its photocatalytic activity," *Journal of Solid State Chemistry*, vol. 180, no. 7, pp. 2080–2087, 2007.

[24] T. A. Egerton, "Uv-absorption-the primary process in photocatalysis and some practical consequences," *Molecules*, vol. 19, no. 11, pp. 18192–18214, 2014.

[25] M. Zhang, T. An, X. Liu, X. Hu, G. Sheng, and J. Fu, "Preparation of a high-activity ZnO/TiO2 photocatalyst via homogeneous hydrolysis method with low temperature crystallization," *Materials Letters*, vol. 64, no. 17, pp. 1883–1886, 2010.

[26] R. Wang, X. Xu, Y. Zhang, Z. Chang, Z. Sun, and W.-F. Dong, "Functionalized ZnO@TiO2 nanorod array film loaded with ZnIn0.25Cu0.02S1.395 solid-solution: synthesis, characterization and enhanced visible light driven water splitting," *Nanoscale*, vol. 7, no. 25, pp. 11082–11092, 2015.

[27] A. Van Dijken, A. H. Janssen, M. H. P. Smitsmans, D. Vanmaekelbergh, and A. Meijerink, "Size-selective photoetching of nanocrystalline semiconductor particles," *Chemistry of Materials*, vol. 10, no. 11, pp. 3513–3522, 1998.

[28] B. Neppolian, H. C. Choi, S. Sakthivel, B. Arabindoo, and V. Murugesan, "Solar/UV-induced photocatalytic degradation of three commercial textile dyes," *Journal of Hazardous Materials*, vol. 89, no. 2-3, pp. 303–317, 2002.

[29] N. Serpone, P. Maruthamuthu, P. Pichat, E. Pelizzetti, and H. Hidaka, "Exploiting the interparticle electron transfer process in the photocatalysed oxidation of phenol, 2-chlorophenol and pentachlorophenol: chemical evidence for electron and hole transfer between coupled semiconductors," *Journal of Photochemistry and Photobiology, A: Chemistry*, vol. 85, no. 3, pp. 247–255, 1995.

[30] W. Smith and Y. P. Zhao, "Superior photocatalytic performance by vertically aligned core-shell TiO_2/WO_3 nanorod arrays," *Catalysis Communications*, vol. 10, no. 7, pp. 1117–1121, 2009.